Cryogenic silicification of microorganisms in hydrothermal fluids

Mark G. Fox-Powell[1,2], Alan Channing[3], Daniel Applin[4], Ed Cloutis[4], Louisa J. Preston[5] & Claire R. Cousins*[1,2]

[1]*School of Earth and Environmental Sciences, University of St Andrews, Irvine Building, North Street, St Andrews, Fife, UK, KY16 9AL.*

[2]*St Andrews Centre for Exoplanet Science, University of St. Andrews, UK*

[3]*School of Earth and Ocean Sciences, Cardiff University, Cardiff, Wales, UK, CF10 3AT.*

[4]*Department of Geography, University of Winnipeg, Winnipeg, MB, Canada R3B 2E9.*

[5]*Department of Earth and Planetary Science, Birkbeck, University of London, Malet St., Bloomsbury, London, UK*

*Corresponding author: crc9@st-andrews.ac.uk

ABSTRACT

Silica-rich hydrothermal fluids that experience freezing temperatures precipitate cryogenic opal-A (COA) within ice-bound brine channels. We investigated cryogenic silicification as a novel preservation pathway for chemo- and photo-lithotrophic Bacteria and Archaea. We find that the co-partitioning of microbial cells and silica into brine channels causes microorganisms to become fossilised in COA. Rod- and coccoidal-form Bacteria and Archaea produce numerous cell casts on COA particle surfaces, while *Chloroflexus* filaments are preserved inside particle interiors. COA particles precipitated from natural Icelandic hot spring fluids possess similar biomorphic casts, including those containing intact microbial cells. Biomolecules and inorganic metabolic products are also captured by COA precipitation, and are detectable with a combination of visible - shortwave

infrared reflectance, FTIR, and Raman spectroscopy. We identify cryogenic silicification as a newly described mechanism by which microbial biosignatures can be preserved within silica-rich hydrothermal environments. This work has implications for the interpretation of biosignatures in relic hydrothermal settings, and for life-detection on Mars and Enceladus, where opaline silica indicative of hydrothermal activity has been detected, and freezing surface conditions predominate.

KEYWORDS: Cryogenic Opal-A; silicification; microfossils; biosignatures; hydrothermal

1. INTRODUCTION

Opaline silica (opal-A) has been a common preservation agent for microorganisms throughout the Earth's geological record[1,2], and is found in many neutral-alkaline hydrothermal systems worldwide. Precipitated by the cooling of aqueous hydrothermal solutions, colloidal silica is widely observed to mineralise microbial cells[1,3] and mats, and associated organic material[4] in modern-day siliceous hot spring environments. Ambient temperature groundwater springs are also capable of precipitating silica and entombing microbes, preserving them as microfossils[5], and relic Archaean hot spring silica sinters may preserve some of the oldest evidence for life on Earth[6]. This physical capturing and subsequent silicification of microbial biosignatures makes opaline silica an attractive target material in the search for life beyond Earth, namely on Mars, and icy moons (i.e. Europa and Enceladus)[2,7].

Opal-A has been observed on Mars[8–11] in association with volcanic centres[10] and hydrovolcanic structures[12], while one of the shortlisted landing sites for the NASA Mars 2020 rover includes a relic hydrothermal system bearing opal-A deposits[9,13]. Recent detections of colloidal silica associated with Enceladus[14], and molecular hydrogen within the Enceladan cryovolcanic plumes[15] offer the strongest evidence to date for ongoing hydrothermal activity on another planetary body, and suggests that the liquid water sourcing these plumes has conditions suitable for biological methanogenesis[15,16]. The sub-freezing surface temperatures that have prevailed on Mars for much of its history[17], and characterise present-day conditions on icy moons,

mean that silicification mechanisms will differ from those typically observed on Earth. This has direct implications for the preservation of any resident microorganisms and their biosignatures.

Under non-freezing conditions, silica-chloride hot springs precipitate siliceous sinters through the cooling of hot (>100 °C) silica-supersaturated hydrothermal fluids, which leads to the nucleation and eventual sedimentation of colloidal silica. When warm hydrothermal fluids are discharged into a freezing environment, the crystallisation of water as ice accelerates the precipitation of colloidal silica, which is forced into brine veins in between ice crystals, along with dissolved solutes (such as Na^+ and Cl^-)[18]. The result is the precipitation of cryogenic opal-A (COA) particles with distinctive morphologies defined by the physical dimensions within the brine veins[18]. Microorganisms are known to partition into brine vein networks in ice, exploiting them as a liquid water microenvironment[19]. However, the fate of microorganisms when opal-A precipitates within these brine channels has not been previously investigated. Terrestrial environments where both silica and microorganisms can be co-partitioned during ice formation are found in geothermal regions in Iceland and Yellowstone National Park (USA) where the air temperature is seasonally sub-zero °C for >50% of the year[18,20], and in high altitude geothermal systems such as El Tatio (Chile)[21]. Silicified microorganisms associated spatially with COA particles from Iceland have been previously observed[3], however without any prior demonstration of silicification under cryogenic conditions, it is not possible to ascertain whether they formed cryogenically or during subsequent mineralisation under non-freezing conditions. Here, we combine an examination of natural COA samples from Iceland with experimental cyrosilicification of microorganisms to investigate the preservation (or lack thereof) for microorganisms and associated spectral biosignatures during freezing of silica-rich hydrothermal fluids.

2. MATERIALS AND METHODS

2.1. Microbial strains and growth conditions

Four previously described microbial strains were selected to experimentally test the process of microbial cryosilicification. The strains were chosen primarily to capture a range of morphological, metabolic and phylogenetic diversity representative of microorganisms found across a diverse range of hydrothermal systems[22-24], with an emphasis on readily-cultivable strains isolated from high-temperature neutral-alkaline environments. Where possible, strains isolated from hydrothermal systems were used. Strains included (*i*) the thermophilic sulfate-reducing bacterium *Thermodesulfovibrio islandicus* DSMZ-12570[25], (*ii*) the thermophilic methanogenic archaeon *Methanoculleus thermophilus* DSMZ-2373[26], (*iii*) the filamentous anoxygenic phototroph *Chloroflexus aurantiacus* DSMZ-635[27], and (iv) the photoferrotrophic bacterium *Rhodopseudomonas palustris* TIE-1[28]. *R. palustris* grows readily with either Fe^{2+} or acetate as an electron donor for phototrophy, thus batches cultivated on both substrates were used in experiments to assess differences in silicification and resulting biosignatures for these different metabolic pathways. Growth media and conditions were all as described previously[25–28], with the exception of *C. aurantiacus*, which was cultivated under natural daylight in a clear-fronted incubator rather than under the recommended 1000 lux. This resulted in slower growth but no discernible difference to cellular morphology.

2.2. Experimental silicification

Sodium metasilicate ($Na_2SiO_3.5H_2O$) was dissolved in deionized water to create a synthetic "hydrothermal" fluid at 500 ppm Si, similar to that used for previous cryogenic opal-A experiments (450 ppm Si[18]), and also to concentrations found in hot spring fluids at Strokkur (476 ppm dissolved Si[29]) and in Yellowstone National Park (312-654 ppm)[30]. This solution was buffered to pH 7.7 using HCl, and sterilised via 0.22 µm filtering. Cultures of microorganisms were harvested by centrifugation (10,000× g for 15 minutes), washed once in phosphate-buffered saline (130 mM NaCl, 1 mM NaH_2PO_4, 9 mM Na_2HPO_4, pH 7.7), and once in

sterile 500 ppm silica solution. Washed cells were resuspended in sterile 500 ppm silica solution that had been preheated to 55 °C. An aliquot of sterile 500 ppm silica solution served as an experimental blank. All experiments were frozen at -20 °C for 24 hours, after which they were thawed and prepared for analysis.

2.3. Field sampling

Fresh, naturally-formed cryogenic silica gels were collected from frozen hydrothermal fluid on the Strokkur outflow apron, Geysir geothermal area, Iceland (64.312542 °N; 20.300367 °W) in January 2007 following the protocol in Channing and Butler[18]. The Strokkur spring was the focus of sampling as the Geysir spring has become much less active and is no longer continuously discharging fluid. Strokkur hydrothermal fluid geochemistry was comparable to the experimental set-up, with alkaline (pH 8.5) fluids previously characterised by 476 ppm dissolved Si[29]. COA particles were extracted from these fresh gels as with the experimental samples, with further volumes melted and evaporated within sterile petri dishes for visible - shortwave infrared (Vis-SWIR), FTIR, and Raman spectroscopic analysis. Natural hydrothermal fluids and their indigenous microbial communities were also collected for laboratory cyrosilicification. These were collected aseptically from the Strokkur outflow in sterile bottles in February 2017, where the dissolved Si content was 149 ppm (see below); considerably lower than previously measured[29]. These fluids were then frozen at -20°C in the laboratory, and the resulting COA precipitates extracted as described above.

2.4. Determination of dissolved silica concentration

Dissolved silica content of a fluid sample from the Strokkur discharge apron was determined by Inductively Coupled Plasma Optical Emission Spectroscopy (ICP-OES) at the Open University using a Prodigy7 (Teledyne-Leeman) OES system at 250.960 nm. Samples were diluted by a factor of 20 prior to analysis.

2.5. Optical and fluorescence microscopy

For optical microscopy, aliquots of thawed experimental samples and thawed natural fluids were transferred to glass slides and allowed to fully evaporate, before being gently rinsed with 0.22 µm-filtered MilliQ water to remove salt crystals. These were imaged using a Keyence VHX 2000 digital microscope. For fluorescence microscopy, aliquots of defrosted sample were stained with 1× SYBR Gold (Invitrogen), incubated at room temperature in the dark for 15 minutes, and mounted on 25 mm diameter, 0.22 µm pore size black polycarbonate filters. Samples were excited at 490 nm and imaged at 590 nm using an Amscope T600 series epifluorescence microscope.

2.6. Scanning Electron Microscope (SEM) Imaging

Glass microscope slides used for optical microscopic analysis of experimental COA were subsequently gold-coated for SEM analysis. Gold was chosen as coating material due to its suitability for secondary electron (SE) topographic imaging. Experimental COA were imaged at 10 keV using the SE detector of a Carl Zeiss SIGMA HD VP Field Emission SEM at the University of Edinburgh. COA produced from natural Strokkur fluids were imaged at 5 keV using the SE detector of a Carl Zeiss SIGMA VP Field Emission SEM. Aliquots of defrosted natural samples were placed on carbon pad stubs and gold-coated. Naturally precipitated COA from Strokkur gels were imaged using the SE detector of a Phillips XL30 Environmental SEM at 20 keV and a working distance of 10 mm at the University of Cardiff.

2.7. Vis-SWIR reflectance, FTIR, and Raman spectroscopy

Aliquots of defrosted experimental COA (approximately 100 ml) were passed through a 0.22 µm filter to recover COA particles, and rinsed with 0.22 µm-filtered MilliQ water to remove salt crystals. The resulting powders were analysed alongside powdered (dry sieved <45 µm grain size) natural Strokkur COA at the

Planetary Spectrometer Facility, University of Winnipeg. Visible - SWIR (350 to 2500 nm) reflectance spectra were acquired with an Analytical Spectral Devices FieldSpec Pro HR spectrometer in 1.4 nm steps with a spectral resolution of 2 - 7 nm (internally resampled to 1 nm intervals) at a viewing geometry of i=30° and e=0°. A 150 W quartz–tungsten–halogen collimated light source provided incident lighting. Spectra were measured relative to a 99% Labsphere Spectralon® standard and corrected for minor (<2%) irregularities in its absolute reflectance. 500 spectra of the dark current, standard, and sample were acquired and averaged. 1.25 to 25 μm (8000-400 cm^{-1})

Mid-infrared spectra were obtained using a Thermo Scientific Nicolet iS5 FTIR Spectrometer and an Attenuated Total Reflectance (ATR) attachment equipped with a diamond crystal, housed in the Planetary Spectroscopy Laboratory at Birkbeck, University of London. Reflectance measurements, published as absorbance units, were obtained over a spectral range of 500 to 4000 cm^{-1} at a resolution of 4 cm^{-1}. A diamond calibration standard was used and atmospheric water (H_2O) and carbon dioxide (CO_2) subtractions made. No further processing of data (*e.g.*, smoothing or Fourier self-deconvolution) was used, to avoid the introduction of artefacts. Band positions are reported simply as the observed maxima, rather than maxima obtained from second derivations or from curve fits. Six analyses were taken of each powdered sample of COA which were re-homogenised after each spectral acquisition to obtain an accurate spectral profile of the material and its associated organic functional groups.

Raman spectra (175-4000 cm^{-1}) were collected at a resolution of ~4 cm^{-1} at 614 nm with a B&WTek i-Raman-532-S instrument using the automatic integration time function to maximise signal-noise-ratio. Excitation was provided by a 532 nm ~50 mW solid state diode laser. Raman-scattered light was detected by a Glacier™ T thermoelectrically cooled (14 °C) CCD detector. All measurements comprised a dark current spectrum followed by sample measurement, using identical viewing geometry, integration time, and number of averaged spectra. Raman-shift calibration was monitored through measurements of a polystyrene standard.

3. RESULTS

3.1. Cryogenic Opal-A particles

Natural COA particles (from the active Strokkur hot spring, Iceland) and experimental COA particles produced both from natural Strokkur outflow fluids and synthetic high-silica laboratory fluids exhibit the same distinctive particle morphologies identified previously by Channing and Butler[18] and putative COA particles observed in siliceous sediments in Iceland by Jones and Renaut[20]. These included triple junctions (Fig. 1b), terminal tear-drop and bulb morphologies, branched threads and sheets; particles produced via the break-up of the COA lattice (Fig. 1a) following cryogelling[18]. Experimental COA particles produced from both synthetic and natural fluids comprise colloidal silica microspheres and aggregates ~50 nm in diameter.

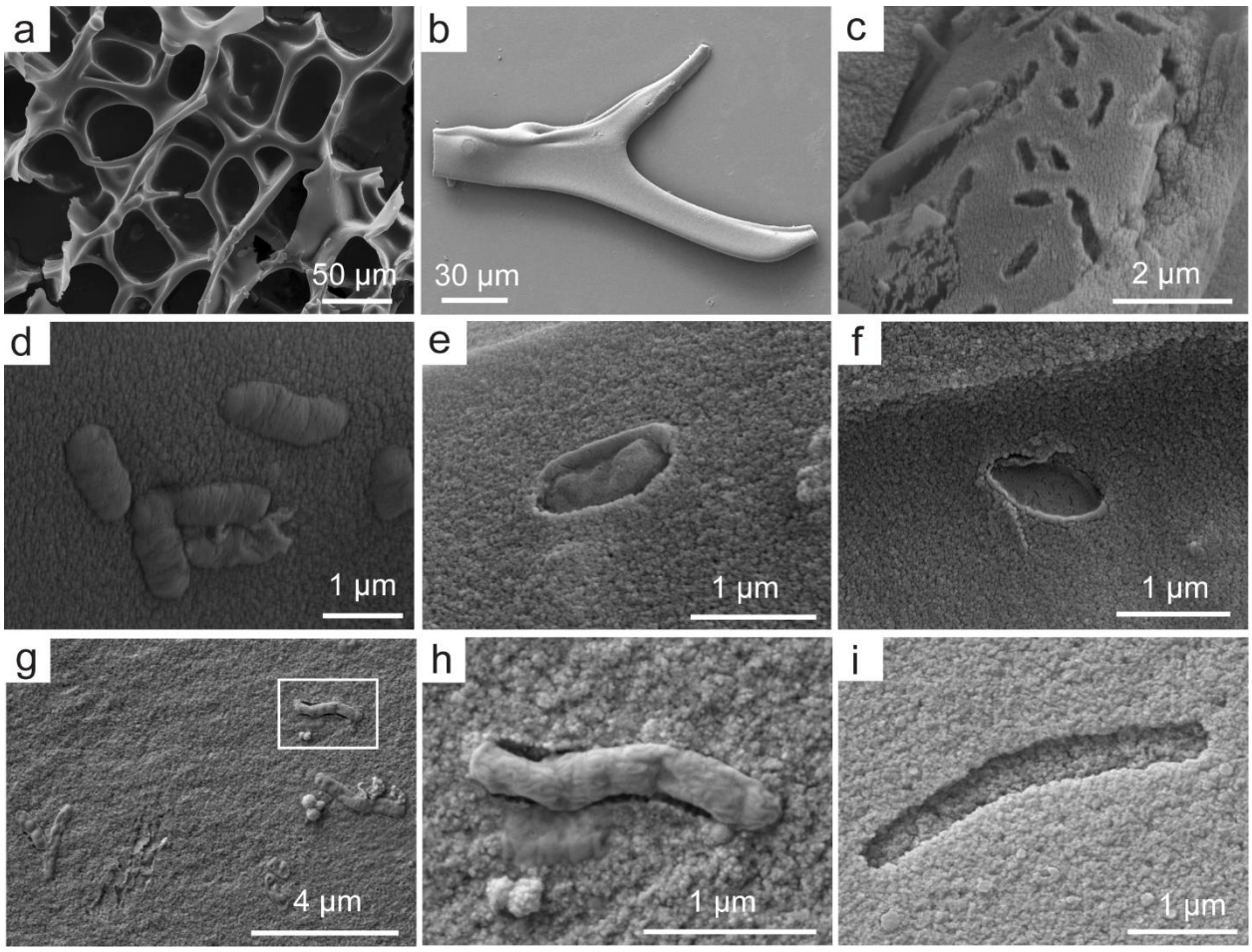

178

179 **Figure 1**. SEM images of experimental and natural COA particles. (*a*) Intact experimental COA lattice. (*b*)
180 COA particle experimentally produced from natural Strokkur fluid, exhibiting triple-junction morphology.
181 (*c*) Experimental COA branch containing cell casts of *Rhodopseudomonas palustris* grown on Fe^{2+}. (*d*)
182 Experimental COA sheet exhibiting fully encased cells of *R. palustris* grown on acetate. (*e*) Cell cast of *M.*
183 *thermophilus* on an experimental COA branch, containing cellular remnants. (*f*) 'Empty' cell cast of *M.*
184 *thermophilus* on an experimental COA branch. (*g*) Experimental COA produced from natural Strokkur fluid
185 exhibiting cellular structures within surface casts. Box indicates region magnified in panel (*h*), showing
186 cellular remnant within surface cast. (*i*) Cast with vibrio cell morphology hosted on COA sheet produced
187 from natural Strokkur fluid.

188

3.2. Microfossils in experimental and natural COA

Our microscopic observations reveal that microbial cells are incorporated into COA particles, becoming completely or partially encased within the colloidal silica matrix. Multiple cell casts are observed on the surface of COA particles and occur along branched threads, at terminal bulbs, and on sheet surfaces (Fig. 1c-i). External casts caused by single cell templating are produced by the photoferrotroph *R. palustris* (Fig. 1c, d) and the methanogenic archaeon *M. thermophilus* (Fig. 1e, f). In both cases, casts preserve their overall cellular morphology. We also observe disintegrated remnants of *M. thermophilus* cells within casts (Fig. 1e) in close proximity to more typical 'empty' casts (Fig. 1f).

Experimental cryogenic silicification of natural fluids from the outflow apron at Strokkur, Iceland, also resulted in the formation of biomorphic casts on the surface of COA particles (Fig. 1g-i). These include casts containing cellular remnants, as observed with *M. thermophilus* (Fig. 1g, h), and empty casts, as observed with *R. palustris* and *T. islandicus* (Fig. 1i). Empty biomorphic cast features are also observed within natural COA particles extracted from gels at Strokkur (Fig. 2a). Other silicified biomorphic features observed in this natural COA include rods or filaments encrusted with opal-A nanospheres in a manner not observed in the experimental samples (Fig. 2b).

The mode of preservation differs between strains. In contrast to the well-preserved cellular morphologies of *R. palustris* and *M. thermophilus*, casts formed by the sulfate-reducing bacterium *T. islandicus* show significant morphological deformities, including shrunken or compressed cell shapes (Fig. 2c) that are unlike the curved-rod 'vibrio' shape of the organisms in culture. Morphological evidence for secondary opal-A crystallisation within casts is also present (Fig. 2c). These deformed cells are also observed on COA particles using epi-fluorescence microscopy (Fig. 2d). Cell casts of the filamentous anoxygenic phototroph *C. aurantiacus* are not observed on COA particle surfaces. Instead, the filamentous cells are incorporated within the interior of COA particles, as revealed by optical and fluorescence microscopy (Fig. 2e-g).

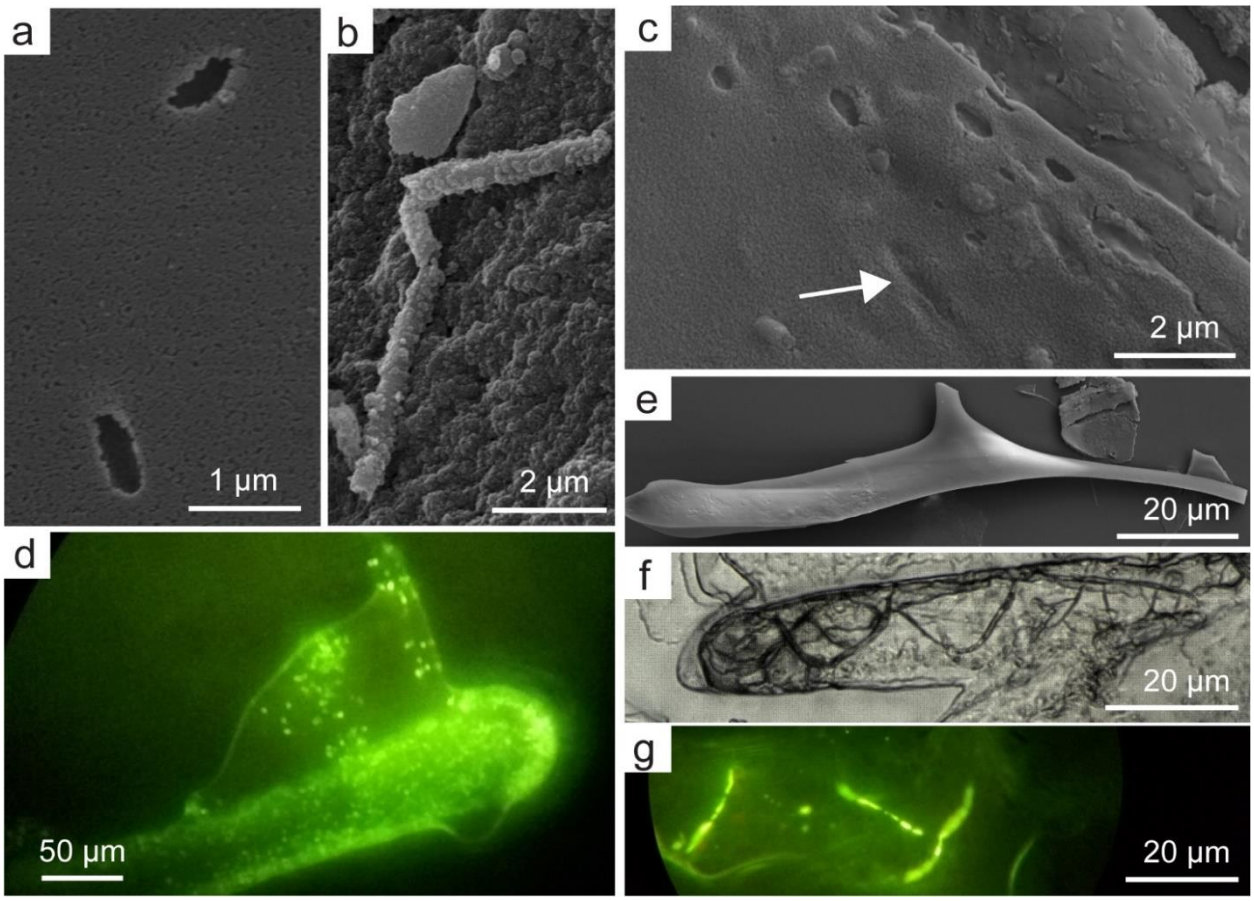

Figure 2. SEM, light, and fluorescence microscope images of experimental and natural COA. (*a*) Biomorphic cell casts on the surface of a natural COA particle collected from Strokkur. (*b*) Possible microbial filament encrusted with opal-A microspheres from natural Strokkur COA. (*c*) Small and deformed cell casts of *T. islandicus*, with possible secondary infilling of earlier cast structures (arrow). (*d*) Fluorescence microscope image of *T. islandicus* COA bulb particle with similarly deformed cells distributed across the particle surface. (*e-g*) COA particles containing cells of *C. aurantiacus*. Note the absence of cellular microfossils at the surface of the large COA particle in SEM image (*e*), whilst filaments are clearly visible within transparent COA particles under both optical (*f*) and fluorescence microscopy (*g*).

3.3. Spectroscopic characterisation of natural and experimental COA

We observe characteristic SWIR spectral features for opal-A, as well as for organic molecules (visible, FTIR, Raman), and inorganic and biomolecular signatures of microbial metabolism (Vis-SWIR) (Fig 3a-c respectively).

3.3.1. Vis-SWIR reflectance

The SWIR reflectance spectra of all experimentally produced and natural COA particles show characteristic absorption bands for hydrated opal-A, including hydration bands at 1.41 and 1.46 µm (interstitial or lattice-bound water; Fig. 3a), water trapped within Si-cages (deep 1.9 µm absorption[31]), and the Si-OH double absorption feature is observed at 2.21 and 2.26 µm[31]. Rice et al.[31] previously showed that hydrated silica phases can be discriminated by comparing the depth and band minimum positions of SWIR hydration bands. Applying band ratio analyses, we show that the experimental and natural COA spectra cluster as a distinct population between the "opal, sinter, and synthetic" silica and "dehydrated sinter" fields[31] (Fig. 4a). Furthermore, natural Strokkur COA particles plot closer to more crystalline phases than the purely experimental COA (Fig. 4b), and exhibit less hydration (Fig. 4c). Based on a comparison of the 1.41 and 1.91 µm band depths, experimentally-produced COA exhibits a range of water contents (Fig. 4c).

All experimental COA samples, including those produced from natural fluids, and the Strokkur COA particulates, have a number of additional absorption features in the visible spectral region that are absent in the experimental blank COA. Absorption bands of light-harvesting pigments bacteriochlorophyll *a* (590, 805 and 871 nm) and bacteriochlorophyll *c* (670 nm) are observed in COA containing *C. aurantiacus*, and *R. palustris* (grown with acetate as the electron donor), and bacteriochlorophyll *c* peaks are also detectable in COA experimentally produced from Strokkur fluids and the natural COA particles collected from Strokkur (Fig. 3a). COA containing *R. palustris* (grown with Fe^{2+} as the electron donor) is characterised by fewer bacteriochlorophyll bands (805 and 871 nm only), and instead exhibits a steep ferric absorption edge between 400 – 700 nm, consistent with the presence of iron (oxyhydr)oxides. Finally, COA containing the

sulfate reducing bacterium *T. islandicus* shows a characteristic steep sulfur absorption between 350 – 550 nm, and a broad Fe^{2+} absorption centred at 1000 nm, consistent with the presence of iron sulfide.

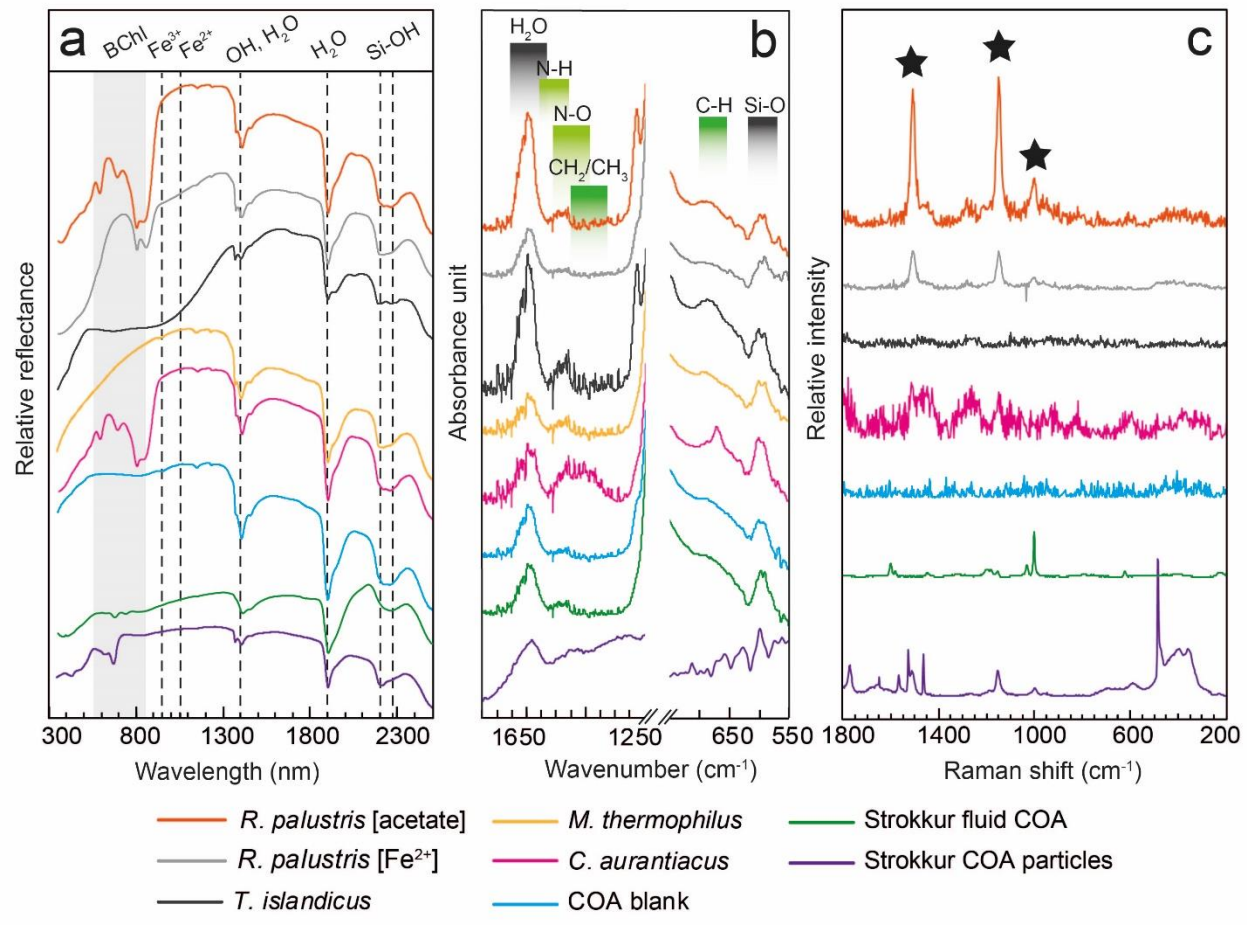

Figure 3. Spectroscopic analysis of experimental and natural COA with band regions and major peaks identified. (*a*) visible – SWIR reflectance spectra showing absorption bands in the visible for bacteriochlorophyll pigments (BChl) and inorganic phases (dashed lines). (*b*) FTIR spectra showing absorption peaks relating to inorganic phases and organic functional groups. A large Si-O-Si asymmetric stretch feature at approx. 1051 cm^{-1} in all samples has been removed for clarity. (*c*) Raman spectra with background fluorescence removed showing peaks for β-carotene (black star). Note *M. thermophilus* is not included for clarity due to large background fluorescence.

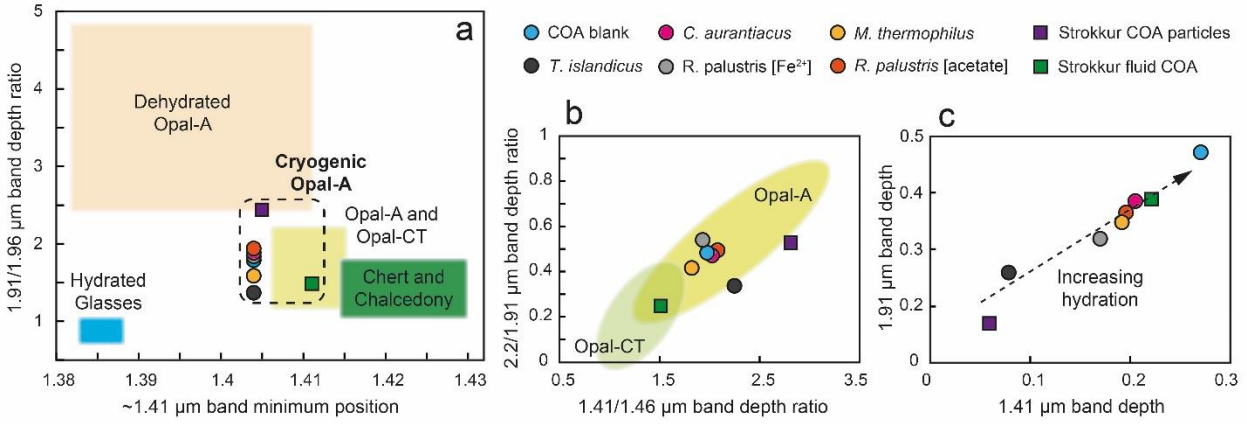

259

260 **Figure 4.** Band parameter plots from Rice *et al.*[31] using SWIR reflectance bands at 1.91, 1.96, 1.41, 1.46,
261 and 2.2 µm to characterise natural COA particles from Strokkur and laboratory-produced COA from natural
262 Strokkur fluid (squares), and experimental COA with and without microorganisms (circles).

263

264 *3.3.2. FTIR Spectroscopy*

265 The FTIR spectra of both natural and experimental COA show absorption bands indicative of organic
266 compounds, including an amine N-H bend between 1520 and 1600 cm^{-1} for COA containing *R. palustris*
267 (grown on acetate), *T. islandicus* and *C. aurantiacus*; alkane CH_2 or CH_3 bending vibrations centred at 1450
268 cm^{-1} exhibited prominently by *C. aurantiacus* COA; and an N-O asymmetric stretch centred at 1500 cm^{-1}
269 for *M. thermophilus* COA and the natural COA particles collected from Strokkur (Fig. 3b). An alkene-
270 related C-H bending vibration centred at 670 cm^{-1} is also observed in COA containing *R. palustris* (grown
271 on acetate), *T. islandicus*, and *C. aurantiacus*. Inorganic hydrated opal-A features at 1650 cm^{-1} and 600 cm^{-1}
272 are observed for all samples (Fig. 3b).

273

274 *3.3.3. Raman Spectroscopy*

275 Raman spectra from natural COA display a broad Si-O-Si peak between 350 – 500 cm^{-1} that is absent in
276 the experimental COA, but peaks for α-quartz (~465 cm^{-1}), meta-stable moganite (~502 cm^{-1}), or

277 paracrystalline opal-C (~777 cm^{-1}) and opal-CT (421 cm^{-1})[32,33] are not observed. An additional, unidentified
278 peak at 490 cm^{-1} is also present in the natural sample. Beyond 800 cm^{-1} *R. palustris* COA and Strokkur
279 COA exhibit β-carotene peaks (Fig. 3a) at 1518, 1155, and 1003 cm^{-1} [34]. Pigment peaks are absent in *C.*
280 *aurantiacus* COA.

281

282 ## 4. DISCUSSION

283 ### 4.1. Cryosilicification of microorganisms

284 Our experiments demonstrate that cryogenic precipitation of opal-A can preserve morphological and
285 geochemical evidence of microorganisms in the resulting COA particles. As the fluid freezes, initial
286 nanoparticle nucleation (≥ 8 nm[35]) is proceeded by rapid COA aggregation between ice crystals as
287 temperature drops below 0° C, trapping microorganisms. Thus, the cryogenic silicification of
288 microorganisms differs from silicification under non-freezing conditions where gradual nanoparticle
289 growth and sinter sedimentation dominate[36]. Similar biomorphic microfossils were observed in the pure-
290 strain experimental COA, experimental COA produced from natural Strokkur fluids and in natural COA
291 particles collected from Strokkur (Fig. 1, 2), providing strong evidence that the encapsulation of
292 microorganisms in this manner is active in nature. Furthermore, the production of COA particles from
293 natural Strokkur fluids, despite a lower initial Si content compared to the experimental fluids (149 ppm vs.
294 500 ppm), demonstrates that this process occurs across a range of silica concentrations. Observation of cell
295 remnants *in situ* within casts produced by *M. thermophilus* and in COA produced from natural Strokkur
296 fluids (Fig. 1e, g, h) suggests large cellular structures such as membranes and/or cell walls can be captured
297 within COA surface casts and ultimately silicified.

298 By experimenting with model microbial strains we also show that the mechanics of microbial
299 cyrosilicification can vary, and in the first instance appear to be controlled by cell morphology. Strains with
300 curved-rod (*T. islandicus*, *R. palustris*) or irregular coccoid (*M. thermophilus*) cell morphology produce

casts on the surface of COA particles, suggesting individual cells are 'sandwiched' between the growing ice crystal face and increasing volume of COA aggregates. Observing these features in COA produced from natural fluids (Fig. 1g-i) demonstrates that the trapping of cells in this manner is active in nature. However, the absence of cell casts for *C. aurantiacus* on COA particle surfaces shows that surficial casting is not the sole mechanism of preservation. Instead, filamentous bacteria (e.g. *C. aurantiacus*) may only be preserved when entirely encased within COA particles (Fig. 2e-g). The absence of bacteriochlorophyll or β-carotene peaks in the *C. aurantiacus* COA Raman spectrum (Fig. 3) is consistent with this, whereby pigments trapped within the translucent COA matrix are detectable using reflectance spectroscopy, but not via surface excitation and Raman scattering.

Functional groups on the surface of microbial cells can act as nucleation sites for opal-A under non-freezing precipitation[37], despite this process being inefficient when compared with spontaneous (abiotic) silica growth[38]. *C. aurantiacus* is unique amongst our experimental strains in that it grows in sheathed filamentous colonies, and the cell wall stains Gram-negative but carries Gram-positive traits such as a single lipid layer and S-layer protein[39]. Whether these characteristics contribute to active silica nucleation is unclear, but our data suggest that *C. aurantiacus* is more efficient at initiating COA precipitation around its entire cell mass, relative to the other microorganisms investigated. The morphologies of our experimental microfossils are otherwise consistent with their corresponding microbial strains, with the sole exception of casts produced by *T. islandicus*, which underwent physical deformation during the cryogelling process (Fig. 2c). The identification by epi-fluorescence microscopy of numerous DNA-bearing cells of a similar size, shape and distribution to the *T. islandicus* casts observed by SEM attests to their biogenicity (Fig. 2d). Finally, all experimental COA fossilising microorganisms shows a shift in the 1.91/1.96 µm SWIR ratio (both positive and negative - Fig. 4a), with no corresponding change to the 1.41 µm band minima position. As the 1.96 band is attributable to the presence of free water molecules[31], this characteristic shift, as well as the broad spread in water content revealed by comparing the 1.41 and 1.91 µm band depths (Fig. 4c) can be explained by the retention of water molecules to differing degrees by captured microorganisms.

4.2. Cryosilicification vs. Non-cryogenic Silicification

By documenting microbial silicification under fully cryogenic conditions, these data provide new insights relating to the preservation of biological activity in hydrothermal systems that experience freezing temperatures. For example, our results contrast with previous investigations into microbial silicification at low temperatures. Westall et al.[40] showed that after a week at 4 °C, many microorganisms (including diatoms, fungi and bacteria) were not silicified, and even after four weeks several bacterial strains remained unsilicified. The precipitation of opal-A on and around microbes in this experiment was characterised by the gradual growth of silica sheaths surrounding cells, and the formation of silica spheroids of up to 2 μm in diameter[40]. Evidence for similar silicification mechanisms were also observed at low temperatures in deep sea environments[41]. These low-temperature studies show similarity to mechanisms described at higher temperatures, both in nature[3] and in the laboratory[33], where gradual sedimentation of large spheroids and the precipitation of cell sheaths dominate the silicification processes. However, in the current study, small (~50 nm; Fig. 1) COA spheroids rapidly formed surface casts or entirely encased microorganisms. Our experiments therefore show that the formation of ice crystals distinguishes this cryogenic process from non-freezing silicification, even when silicification is occurring at low temperatures. Specifically, the formation of concentrated siliceous brines is necessary to drive the precipitation of COA and subsequent capture of microorganisms.

In nature, it is likely that both non-freezing and cryogenic silicification processes are occurring simultaneously. Natural particles with cryogenic morphologies from Strokkur, Iceland, exhibited filamentous biogenic structures encrusted in larger opal-A nanospheres in a manner akin to those observed in previous non-freezing silicification studies[40,41] (Fig. 2b), as well as the smaller COA nanospheres and biomorphic casts typical of experimental COA (Fig. 2a). Silicified microorganisms previously reported in spatial association with natural COA particles in Iceland[20] were encrusted with relatively large spheroids (~2 μm[20]), whilst the COA particles themselves lacked visible cell casts. Viewed in the context of our

observations, these features are suggestive of non-freezing silicification and imply that these microorganisms were silicified under different conditions from the formation of the COA.

On Earth, mid-to-high-latitude and high-altitude hydrothermal systems can experience prolonged sub-zero °C air temperatures[20,21], promoting prolific COA formation. In such localities, cryogenic and non-freezing silicification mineralise different portions of the microbial consortia, whereby the latter predominantly captures biofilms, streamer communities and other benthic organisms[42]. Conversely, cryogenic silicification is likely to more efficiently capture the planktic microorganisms present in the fluid-phase, where ice-formation primarily occurs. Unconsolidated COA particles can become cemented by summer-time sinter development, with the distinctive shape of COA particles identifiable even within reworked sediments[20], but in environments with little to no summertime sinter growth, COA particles are free to be exported when the ice matrix thaws[18]. Under these circumstances, the retention of cells within COA raises questions about whether cells can remain viable following rapid cryosilicification, as has been observed for organisms under non-cryogenic conditions[43]. If so, dispersal of microorganisms within COA particles may have ecological significance in hydrothermal settings.

4.3. Relevance to Mars and icy moons

The recent discovery of both colloidal silica and H_2 being erupted from within Enceladus[14,15] means the subsurface environment could be habitable for simple methanogenic organisms, and that such organisms might be cryogenically silicified in a similar manner to that shown here. Such processes should be further investigated with specific relevance to future surface exploration of Enceladus and other icy moons, such as Europa. Closer to home, one of the shortlisted landing sites for NASA's Mars 2020 rover (Columbia Hills) includes relic hydrothermal systems, and confirmed deposits of opal-A[11]. As vast areas of the Martian surface have experienced persistent freezing temperatures for much of its history[44,45], it is likely that the surface discharge of subsurface silica-rich hydrothermal fluids would lead to COA precipitation, trapping

some portion of any putative subsurface Martian microbiota within these COA deposits. Moreover, upcoming Mars surface missions will be equipped with SWIR reflectance spectroscopy (NASA Mars 2020 and ESA ExoMars 2020). We show here that COA deposits would feasibly be identifiable and distinguishable from other amorphous or hydrated silica phases using such instrumentation (Fig. 4), with a broad range of hydration also observed across the experimental and natural samples (Fig. 4c). However, these spectral features are likely to become less pronounced with prolonged exposure to the desiccating atmospheric conditions on Mars. Likewise, the presence of a broad Raman peak between 300 – 500 cm^{-1} in the natural COA particles (Fig. 3a) suggests that freshly-precipitated, unstable COA will eventually develop into more ordered states where energy is available to drive this kinetic process, consistent with the development of other silica sinter deposits[46].

4.4. Spectral detection of biosignatures

Consistent with previous works[47], the spectral detection of non-pigmented biomass in geological substrates remains challenging. The most prominent biomolecular features in the vis-SWIR and Raman spectra are photosynthetic pigments (Fig. 3a), and organic molecule-related absorption features detected in FTIR spectra are minor in comparison to silica-related features, despite the considerable biomass observed with microscopic methods in the experimental samples (Fig. 2d, g). Whilst specialised pigments such as bacteriochlorophyll are unlikely to exist beyond Earth, they serve to demonstrate the capacity of COA formation in the capture of functional biological molecules, and the utility of combined Raman and Vis-SWIR reflectance spectroscopy in the characterisation of such deposits on extraterrestrial surfaces such as Mars and icy moons. Recent work by Dos Santos et al.[48] revealed variation in the UV-shielding effects of minerals on amino acids, while opal-A sinters can be effective absorbers of UV-C and UV-B within the top 1 mm of substrate[49]. Furthermore, previous studies of biomolecule preservation[50] have indicated that, over geological time, the observation of amide absorption bands within rocks and minerals decreases, whereas hydrocarbons such as those detected by FTIR here are more persistent. The ability of COA to effectively

shield biomolecules, or any other captured organics, from other damaging forms of surface radiation and oxidative reactions over representatively long time periods remains to be determined. Similarly, the longevity of COA deposits and cryogenically-generated microfossils in the terrestrial rock record is unknown. However this study demonstrates that investigations of this sort are now required, as they would further define the importance of COA as target phase for extraterrestrial exploration. Likewise, quantifying the effects of different freezing rates, initial fluid temperatures, and the presence of other solutes on the efficiency of cryogenic silicification should constitute future studies.

Acknowledgements

This work was supported by The Carnegie Trust (REF: 70335), The Leverhulme Trust (REF: RPG-2016-153), and a Royal Society of Edinburgh research fellowship to CRC. EAC thanks the Canadian Space Agency, the Natural Sciences and Engineering Research Council of Canada, the Canada Foundation for Innovation, the University of Winnipeg, and the Manitoba Research Innovations Fund for supporting the University of Winnipeg's Planetary Spectrophotometer Facility. The authors thank the National Energy Authority (Orkustofnun) in Iceland for a research permit allowing microbiology research to be conducted at Geysir, and the Iceland Institute of Natural History for permission to export the samples. ICP-OES data from an Icelandic fluid sample was acquired by Timothy Barton and Nisha Ramkissoon of the Open University.

Author contributions

MGFP led and conducted all experimental work, collection of all imaging data for experimental samples, interpretation of data, and authorship of the manuscript. CRC led the study, contributed to the collection and interpretation of data, and co-authored the manuscript. AC collected natural cryogenic opal-A samples from Iceland, associated SEM data, and contributed to the interpretation of data. DA and EAC collected

vis-SWIR and Raman spectroscopic data and contributed to their interpretation. LJP collected FTIR spectroscopic data and contributed to their interpretation.

Competing financial interests: All authors declare that they do not have any competing financial interests.

5. REFERENCES

1. Cady, S. L. & Farmer, J. D. in *Evolution of hydrothermal ecosystems on Earth (and Mars?)* (eds. Bock, G. R. & Goode, J. A.) 150–173 (Wiley, 1996).

2. Westall, F. *et al.* Biosignatures on Mars: What, Where, and How? Implications for the Search for Martian Life. *Astrobiology* **15,** 998–1029 (2015).

3. Jones, B., Renaut, R. & Rosen, M. Taphonomy of Silicified Filamentous Microbes in Modern Geothermal Sinters: Implications for Identification. *Palaios* **16,** 580–592 (2001).

4. Preston, L. J., Benedix, G. K., Genge, M. J. & Sephton, M. A. A multidisciplinary study of silica sinter deposits with applications to silica identification and detection of fossil life on Mars. *Icarus* **198,** 331–350 (2008).

5. Grasby, S. E., Bezys, R. & Beauchamp, B. Silica Chimneys Formed by Low-Temperature Brine Spring Discharge. *Astrobiology* **9,** 931–941 (2009).

6. Djokic, T., Kranendonk, M. J. Van, Campbell, K. A., Walter, M. R. & Ward, C. R. Earliest signs of life on land preserved in ca. 3.5 Ga hot spring deposits. *Nat. Commun.* **8,** (2017).

7. Ruff, S. W. & Farmer, J. D. Silica deposits on Mars with features resembling hot spring biosignatures at El Tatio in Chile. *Nat. Commun.* **7,** 1–10 (2016).

8. Milliken, R. E. *et al.* Opaline silica in young deposits on Mars. *Geology* **36,** 847–850 (2008).

9. Squyres, S. W. *et al.* Detection of Silica-Rich Deposits on Mars. *Science (80-.).* **320,** 1063–1067

(2008).

10. Skok, J. R., Mustard, J. F., Ehlmann, B. L., Milliken, R. E. & Murchie, S. L. Silica deposits in the Nili Patera caldera on the Syrtis Major volcanic complex on Mars. *Nat. Geosci.* **3,** 838–841 (2010).

11. Ruff, S. W. *et al.* Characteristics, distribution, origin, and significance of opaline silica observed by the Spirit rover in Gusev crater, Mars. *J. Geophys. Res. E Planets* **116,** (2011).

12. Rice, M. S. *et al.* Silica-rich deposits and hydrated minerals at Gusev Crater, Mars: Vis-NIR spectral characterization and regional mapping. *Icarus* **205,** 375–395 (2009).

13. Farley, K. A. & Williford, K. H. *Report on the outcomes of the third Mars 2020 Landing Site Workshop*. (2017).

14. Hsu, H.-W. *et al.* Ongoing hydrothermal activities within Enceladus. *Nature* **519,** 207–210 (2015).

15. Waite, J. H. *et al.* Cassini finds molecular hydrogen in the Enceladus plume: Evidence for hydrothermal processes. *Science (80-.).* **356,** 155–159 (2017).

16. Taubner, R.-S. *et al.* Biological methane production under putative Enceladus-like conditions. *Nat. Commun.* **9,** (2018).

17. Carr, M. H. & Head, J. W. Geologic history of Mars. *Earth Planet. Sci. Lett.* **294,** 185–203 (2010).

18. Channing, A. & Butler, I. B. Cryogenic opal-A deposition from Yellowstone hot springs. *Earth Planet. Sci. Lett.* **257,** 121–131 (2007).

19. Mader, H. M., Pettitt, M. E., Wadham, J. L., Wolff, E. W. & Parkes, R. J. Subsurface ice as a microbial habitat. *Geology* **34,** 169–172 (2006).

20. Jones, B. & Renaut, R. W. Impact of Seasonal Changes on the Formation and Accumulation of Soft Siliceous Sediments on the Discharge Apron of Geysir, Iceland. *J. Sediment. Res.* **80,** 17–35 (2010).

21. Nicolau, C., Reich, M. & Lynne, B. Physico-chemical and environmental controls on siliceous sinter

formation at the high-altitude El Tatio geothermal field, Chile. *J. Volcanol. Geotherm. Res.* **282,** 60–76 (2014).

22. Skirinisdottir, G., et al. Influence of sulfide and temperature on species composition and community structure of hot spring microbial mats. *Appl. Environ. Microbiol*. **66**, 2835-2841 (2000)

23. Hedlund, B. P., Dodsworth, J. A., Cole, J. K. & Panosyan, H. H. An integrated study reveals diverse methanogens, *Thaumarchaeota* and yet-uncultivated archaeal lineages in Armenian hot springs. *Antonie van Leeuwenhoek* **104**, 71-82 (2013)

24. Akimov, N., Podosokorskaya, O. A., Shlyapnikov, M. G. & Gal, V. F. Dominant phylotypes in the 16S rRNA gene clone libraries from bacterial mats of the Uzon Caldera (Kamchatka, Russia) hydrothermal springs. *Microbiology* **82**, 721-727 (2013)

25. Sonne-Hansen, J. & Ahring, B. K. *Thermodesulfobacterium hveragerdense* sp. nov., and *Thermodesulfovibrio islandicus* sp. nov., two thermophilic sulfate reducing bacteria isolated from a Icelandic hot spring. *Syst. Appl. Microbiol.* **22,** 559–564 (1999).

26. Rivard, C. J. & Smith, P. H. Isolation and characterization of a thermophilic marine methanogenic bacterium, *Methanogenium thermophilicum* sp. nov. *Int. J. Syst. Bacteriol.* **32,** 430–436 (1982).

27. Pierson, B. K. & Castenholz, R. W. A phototrophic gliding filamentous bacterium of hot springs, Chloroflexus aurantiacus, gen. and sp. nov. *Arch. Microbiol.* **100,** 5–24 (1974).

28. Jiao, Y., Kappler, A., Croal, L. R., Newman, K. & Newman, D. K. Isolation and characterization of a genetically tractable photoautotrophic Fe (II) -oxidizing bacterium , *Rhodopseudomonas palustris* strain TIE-1. *Appl. Environ. Microbiol.* **71,** 4487–4496 (2005).

29. Konhauser, K. O. & Ferris, F. G. Diversity of iron and silica precipitation by microbial mats in hydrothermal waters, Iceland: Implications for Precambrian iron formations. *Geology* **24,** 323–326 (1996).

30. Fournier, R. O. Geochemistry and dynamics of the Yellowstone National Park hydrothermal system. *Annu. Rev. Earth Planet. Sci.* **17,** 13–53 (1989).

31. Rice, M. S. *et al.* Reflectance spectra diversity of silica-rich materials: Sensitivity to environment and implications for detections on Mars. *Icarus* **223,** 499–533 (2013).

32. Kingma, K. J. & Hemley, R. J. Raman spectroscopic study of microcrystalline silica. *Am. Mineral.* **79,** 269–273 (1994).

33. Lynne, B. Y., Campbell, K. A., Moore, J. N. & Browne, P. R. L. Diagenesis of 1900-year-old siliceous sinter (opal-A to quartz) at Opal Mound, Roosevelt Hot Springs. *Sediment. Geol.* **179,** 249–278 (2005).

34. Marshall, C. P. & Marshall, A. O. The potential of Raman spectroscopy for the analysis of diagenetically transformed carotenoids. *Philos. Trans. R. Soc. A* **368,** 3137–3144 (2010).

35. Tobler, D. J., Shaw, S. & Benning, L. G. Quantification of initial steps of nucleation and growth of silica nanoparticles: An in-situ SAXS and DLS study. *Geochim. Cosmochim. Acta* **73,** 5377–5393 (2009).

36. Orange, F. O., Lalonde, S. V & Konhauser, K. O. Experimental Simulation of Evaporation-Driven Silica Sinter Formation and Microbial Silicification in Hot Spring Systems. *Astrobiology* **13,** 163–176 (2013).

37. Konhauser, K. O., Jones, B., Phoenix, V. R., Ferris, G. & Renaut, R. W. The Microbial Role in Hot Spring Silicification. *AMBIO A J. Hum. Environ.* **33,** 552–558 (2004).

38. Yee, N., Phoenix, V. R., Konhauser, K. O., Benning, L. G. & Ferris, F. G. The effect of cyanobacteria on silica precipitation at neutral pH: Implications for bacterial silicification in geothermal hot springs. *Chem. Geol.* **199,** 83–90 (2003).

39. Pierson, B. K. & Castenholz, R. W. in *Bergey's Manual of Systematics of Archaea and Bacteria* 1–

16 (John Wiley & Sons, Inc., in association with Bergey's Manual Trust, 2015). doi:10.1002/9781118960608.gbm00380.

40. Westall, F., Boni, L. & Guerzoni, E. The experimental silicification of miroorganisms. *Palaeontology* **38,** 495–528 (1995).

41. Monty, C. L. V., Westall, F. & van der Gaast, S. Diagenesis of siliceous particles in subantarctic sediments, hole 699A: Possible microbial mediation. *Proc. Ocean Drill. Program, Sci. Results* **114,** 685–710 (1991).

42. Schultze-Lam, S., Ferris, F. G., Konhauser, K. O. & Wiese, R. G. In situ silicification of an Icelandic hot spring microbial mat: implications for microfossil formation. *Can. J. Earth Sci.* **32,** 2021–2026 (1995).

43. Phoenix, V. R., Adams, D. G. & Konhauser, K. O. Cyanobacterial viability during hydrothermal biomineralisation. *Chem. Geol.* **169,** 329–338 (2000).

44. Fairén, A. G. A cold and wet Mars. *Icarus* **208,** 165–175 (2010).

45. Wordsworth, R. D., Kerber, L., Pierrehumbert, R. T., Forget, F. & Head, J. W. Comparison of 'warm and wet' and 'cold and icy' scenarios for early Mars in a 3-D climate model. *J. Geophys. Res. Planets* **120,** 1201–1219 (2015).

46. Herdianita, N. R., Browne, P. R. L., Rodgers, K. A. & Campbell, K. A. Mineralogical and textural changes accompanying ageing of silica sinter. *Miner. Depos.* **35,** 48–62 (2000).

47. Gaboyer, F. *et al.* Mineralization and Preservation of an extremotolerant Bacterium Isolated from an Early Mars Analog Environment. *Sci. Rep.* **7,** (2017).

48. Dos Santos, R., Patel, M., Cuadros, J. & Martins, Z. Influence of mineralogy on the preservation of amino acids under simulated Mars conditions. *Icarus* **277,** 342–353 (2016).

536 49. Phoenix, V. R., Bennett, P. C., Engel, A. S., Tyler, S. W. & Ferris, F. G. Chilean high-altitude hot-
537 spring sinters: a model system for UV screening mechanisms by early Precambrian cyanobacteria.
538 *Geobiology* **4,** 15–28 (2006).

539 50. Preston, L. J. *et al.* The preservation and degradation of filamentous bacteria and biomolecules
540 within iron oxide deposits at Rio Tinto, Spain. *Geobiology* **9,** 233–249 (2011).